Risk-based approach for rational categorization of damage observations from wind turbine blade inspections

Dimitrov, Nikolay Krasimirov

Published in:
Journal of Physics: Conference Series

Link to article, DOI:
10.1088/1742-6596/1037/4/042021

Publication date:
2018

Document Version
Publisher's PDF, also known as Version of record

Risk-based approach for rational categorization of damage observations from wind turbine blade inspections

Risk-based approach for rational categorization of damage observations from wind turbine blade inspections

Nikolay Dimitrov[1,2]

[1] DTU Wind Energy, Technical University of Denmark, 4000 Roskilde, Denmark
[2] nkdi@dtu.dk

Abstract. This study provides a risk-based assessment procedure for wind turbine blade damages observed during visual inspections. A decision model is presented which identifies the cost-optimal intervention based on assessed damage severity. This is achieved by defining procedures for model-based estimation of probability of consequences for specific failure modes, and by analysing the costs associated with different scenarios for intervention. In addition, the procedure provides a risk-based, quantitative interpretation of damage severity categories used in wind turbine blade inspection practices. In the present paper, the workflow and example categorization are demonstrated on two specific faults in wind turbine blades: leading edge erosion damage, and trailing edge crack.

1. Introduction

Modern wind turbines are monitored by different means with the intention of detecting faults and evaluating the turbine condition. Once an issue is detected by e.g. a visual inspection, the obtained information has to be analysed to assess the severity of the issue and, based on that, take a decision for the most appropriate corrective action. This process is normally carried out manually based on expert assessment, meaning that it is prone to uncertainty due to subjectivity and incomplete information regarding the consequences. Some aspects of the automatization of this process are taken into consideration by studies as e.g. [1],[2], where optimal strategies for risk-based inspection planning are considered. The main purpose of the present study is to provide a risk-based assessment of observed damage severity and demonstrate how this can be utilized to select an optimal maintenance strategy. This procedure can also act as a supplement to standard inspection-based decision practices employing damage severity categories, by providing a quantitative interpretation and calibration of the damage categories. The problem is considered with a specific focus on wind turbine blade issues detected by optical inspection as achievable by a camera-carrying UAV (drone). The envisioned practice allows assessment of first-time detected issues with the use of damage progression models, as well as updates based on repeated inspections. The following specific objectives are covered in the present study:

- Presenting a quantitative definition of damage severity categories by means of a risk matrix;
- Exemplifying procedures for model-based estimation of probability of consequences for specific failure modes;
- Demonstrating the computation of the risk associated with possible maintenance strategies;
- Outlining a decision model for optimal intervention based on the assessed damage severity.

2. Risk model definition

In engineering risk analysis, the risk associated with a given scenario is defined as the product of the probability of occurrence and the expected consequence [3]. The scenario probabilities are evaluated

quantitatively which allows obtaining numerical risk values which can be categorized in a risk matrix as shown on Figure 1. Since all entries in a given diagonal of the risk matrix correspond to equal risk, they belong to the same risk category, and the size of the matrix can be decided based on the number of risk categories necessary. In the example on Figure 1, there are 5 risk categories which correspond to what is used in industry [4]. In the situation of a damage being detected during an inspection, the severity category of the damage is assessed by computing the overall risk which is the sum of the risks from all possible scenarios for further evolution of the detected issue.

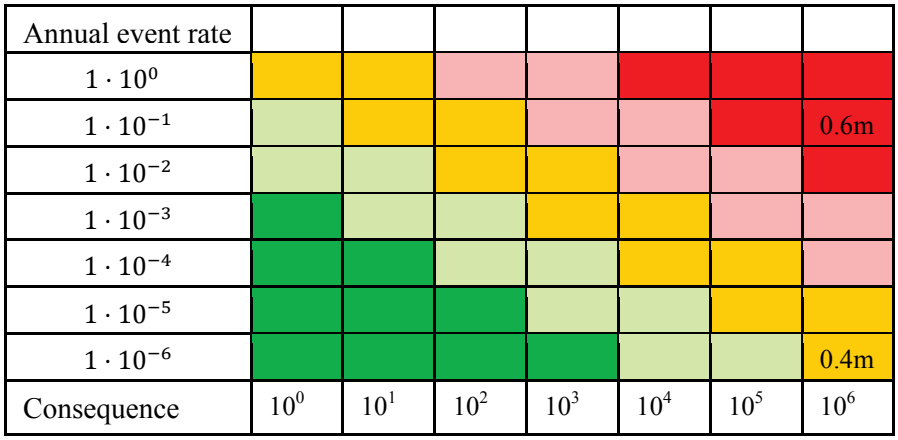

Figure 1. Example risk matrix defining five possible severity categories. The two example entries represent an estimate of the risk for 0.4m and 0.6m long trailing-edge cracks progressing to critical size within one year.

2.1. Event tree formulation

The scenarios for development of damage and the range of consequences are formulated in terms of an event tree, Figure 2. The event tree takes into account both situations where any further deterioration affects directly the performance of the turbine (e.g. leading edge erosion), and situations where the deterioration only affects the likelihood of failure (e.g. a trailing edge crack). The component failure may represent either ultimate failure (and required component replacement) or a requirement for component repair, with the difference between the cases reflected in the magnitude of the consequences.

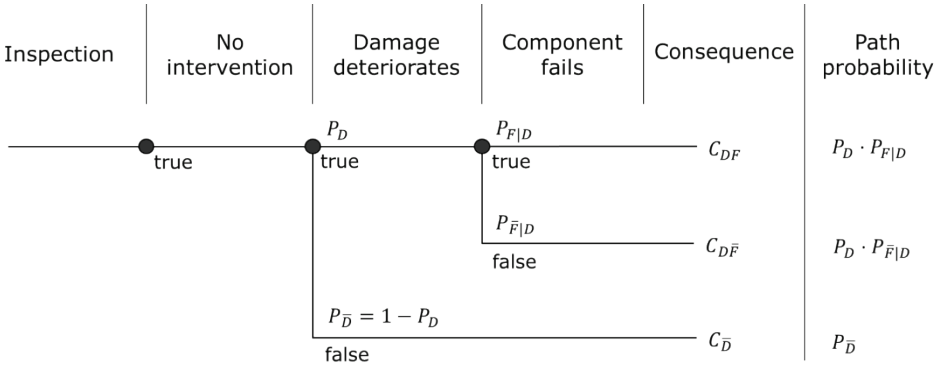

Figure 2. Event tree defining the set of possible consequences conditional on observed damage and no intervention.

The variables introduced in Figure 2 are defined as follows:

- P_D is the probability of deterioration given that no intervention has taken place;
- $P_{F|D}$ is the probability of ultimate failure following deterioration; $P_{\bar{F}|D}$ its complementary;
- C_{DF} is the total consequence (cost) of a component failure after deterioration;
- $C_{D\bar{F}}$ is the consequence of performance loss due to deterioration without ultimate failure;
- $C_{\bar{D}}$ is the consequence of no progress in the deterioration process.

2.2. Failure scenario probabilities

We consider that the degree of deterioration (the loss of performance and structural capacity) of a component can be described as function of time t by a continuous random variable, $D(t)$. In case the deterioration can lead to ultimate failure (e.g. complete loss of function) of the component, the level at which ultimate failure occurs is denoted by D_{cr}. Thus, the probability that failure of a component will occur before a certain time t_{fail} is given by $P_{F|D} = Prob(t_{fail} \leq t) = Prob(D(t) - D_{cr} \geq 0)$. Given the probability distributions of $D(t)$ and D_{cr}, $P_{F|D}$ can be determined using convolution or simple reliability analysis. The deterioration variable $D(t)$ is considered as a cumulative sum of infinitesimal damage increments, $D(t) = \int_{t0}^{t} dD(\mathbf{X}(t_i))\mathrm{d}t$, or in discretized form, $D(t) = \sum_{i=1}^{N\Delta t} \Delta D\big(\mathbf{X}(t_i)\big)$, where $\Delta D\big(\mathbf{X}(t_i)\big)$ is the increment over a time period Δt, and N is the total number of periods. $\mathbf{X}(t)$ is a vector of random variables which can influence the rate of damage accumulation. As a minimum, $\mathbf{X}(t)$ consists of the initial damage size u_d and location z_d, as well as some relevant external factors as e.g. wind speed, wind direction and turbulence.

Given the above definitions, the expected value of $D(t)$ for a sufficiently long period t can be determined as $E[D(t)] = t \cdot E\big[\Delta D\big(\mathbf{X}(t)\big)\big]$. However, characterizing the full probability distribution or at least the variance is not as straightforward, because there typically will be time correlation between different realizations of $\mathbf{X}(t)$ (the wind speed being an obvious example). In such situations it can be more convenient to carry out a Monte Carlo simulation with random damage progression scenarios (Figure 6), which is then used to produce an empirical estimate of the distribution of $D(t)$.

2.3. Computing consequence costs

In order to compute the risk from the considered scenarios, we need to also compute the costs associated with each scenario. For some situations the cost can be considered a constant, but for the cases where deterioration affects performance (power production) the cost will be a function of the time to failure. In the cost definition, we use the following variables:

- $D(t)$ and t_{fail} are the deterioration as function of time, and time to failure respectively;
- t_{lead} is the mobilization time necessary for preparing a corrective action (e.g. time for delivering spare parts and organizing a repair crew);
- t_{repair} is the duration of the repair action;
- $t_{service}$ is the time to next scheduled service campaign;
- T is a reference time period, e.g. could be equal to the time to subsequent inspection;
- $C_r(D(t), z_d)$ is the total cost of replacement or major repair of a certain component – dependent on the damage size $u_d(t) \propto D(t)$ and location z_d;
- $C_{prod}(D(t), t) = \int_0^t \Delta C_{prod}\big(D(t), \mathbf{X}(t)\big)\mathrm{d}t$ is the income from power production which may be progressively affected from deterioration (e.g. as is the case with leading-edge erosion);

Based on these variable definitions, the costs associated with the scenarios given in Figure 2 can be computed as follows:

- $C_{DF} = C_r(D(t), z_d) + \int_0^T f_{t_{fail}} \Big(C_{prod}\big(D(t_{fail}), t_{lead} + t_{repair}\big) + C_{prod}\big(D(t_{fail}), t_{fail}\big)\Big)\,\mathrm{d}t_{fail}$;
- $C_{D\bar{F}} = \int_0^T C_{prod}(D(t), t)\mathrm{d}t$;
- $C_{\bar{D}} = C_{prod}(D = D(0), T)$. (1)

The above cost definitions reflect the scenario of taking a decision that no intervention is carried out within the reference time period, T. The total risk associated with this scenario is computed as

$$\text{Risk(Sc. 1)} = P_D P_{F|D} C_{DF} + P_D P_{\bar{F}|D} C_{D\bar{F}} + P_{\bar{D}} C_{\bar{D}} \quad (2)$$

Other possible decisions are e.g. immediate intervention by stop of the turbine following damage detection, delaying intervention by t_{lead} to prepare the corrective action, or repairing at the next scheduled service. These decisions form separate branches of the event/decision tree, and costs and probabilities are computed in a similar way, using the same set of basic variables defined above.

3. Computing damage growth

3.1. Damage growth computation algorithm

Computing the costs associated with continuous deterioration and component failure requires determining the probability distribution of the deterioration as function of time, as well as the probability of component failure as function of time. This is done in the following steps:

- Define a model which computes the damage increment $\Delta D\big(\mathbf{X}(t_i)\big)$ as function of environmental condition inputs;
- Map the damage increments over the set of environmental conditions **X** using e.g. a surrogate modelling approach;
- Carry out a Monte Carlo simulation to compute the time-dependent distribution of $D(t)$ as well as $C_{prod}(D(t), t)$;
- If complete failure is possible, determine $P_{F|D} = Prob(t_{fail} \leq t) = Prob(D(t) - D_{cr} \geq 0)$, using a simple reliability analysis procedure.

Defining the model for computing damage growth increments is possibly the most challenging task in the above procedure. While the remaining steps in the algorithm may be carried out in a very similar way for different fault types, the damage increment model will be specific to the physics of the particular fault type. Below, examples for the computation of damage growth rates are given for two failure types: leading-edge erosion at the tip of a wind turbine blade, and a crack propagating in the trailing edge of a wind turbine blade. The examples are for demonstration purposes and are based on sources from literature. The results are example, normalized estimations of the damage increments.

3.2. Damage growth rate for leading edge erosion

Blade leading edge erosion (LEE) is the progressive loss of blade coating material at the leading edge due to high-speed collisions with particles contained in the air inflow. According to [5], collisions with rain droplets can cause substantial erosion and the rate of LEE is dependent on the rain intensity I_r, and the prevalent rain droplet size, r. These two quantities can be related by an empirical relationship defined in [6], which gives the probability distribution of the rain drop sizes in mm as function of rainfall intensity in mm/hour. If for any value of I_r a characteristic value r_c is chosen for r so that it is representative of its distribution, the dependence between LEE and rain conditions can be expressed solely in terms of the characteristic values r_c. This can be modelled using a log-linear relationship similar to the S-N curve relationships in fatigue analysis:

$$\log \Delta D = \log K - m \log r_c \tag{3}$$

where m and K are model parameters. The LEE damage is defined as a normalized quantity, where $D = 1$ corresponds to LEE damage resulting in loss of annual energy production (AEP) equal to 3.5%. Under these conditions, based on results from [5] the value of the LEE damage growth parameters are computed as $\log K = 5.726$ and $m = 12.731$, for LEE damage growth per hour, for blade tip speed of 90m/s, and for characteristic rain drop sizes r_c equal to the mean of r conditional on I_r.

The rainfall events are simulated as a Poisson process. The process is characterized with an event rate λ_r which is the mean time between events. Each event is for simplicity considered as a rectangular pulse with random mean intensity I_r and a random duration d_r. The rainfall intensities are modelled using a log-normal distribution (Figure 3) with parameters based on a fit to measurement data for 1h mean intensities for oceanic climates reported in [7]. An example histogram of the mean intensities of simulated rainfall events over a 1-year period is shown on Figure 4. The duration of each event is modelled as exponentially distributed with distribution parameter λ_{d_r}. The rainfall duration and intensity are inversely correlated [8], and in the present study the duration distribution parameter is defined as conditionally dependent on the rainfall intensity with the relation $\log_{10} \lambda_{d_r} = -1.33 \log_{10} I_r$. The resulting joint distribution of I_r and d_r is shown on Figure 5, based on a Monte Carlo simulation of rainfall events over one year. For any simulated event the

characteristic drop sizes r_c are computed from the values of I_r, and subsequently the increment in LEE damage is computed using Equation (3) and multiplying by the event durations d_r. Considering that $D = 1$ is assumed to correspond to 3.5% reduction in AEP, the cumulative damage obtained using a Monte Carlo simulation of rainfall events can be represented as a progressing reduction in AEP. The results from 100 such Monte Carlo simulations with 1-year durations are shown on Figure 6.

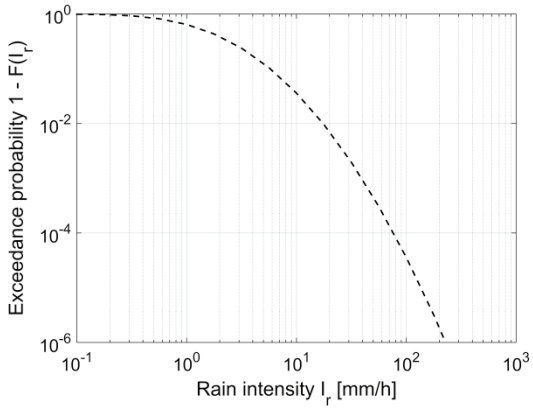

Figure 3. Exceedance probability curve for hourly rain intensities, conditional on the event of rainfall. Based on data from [7].

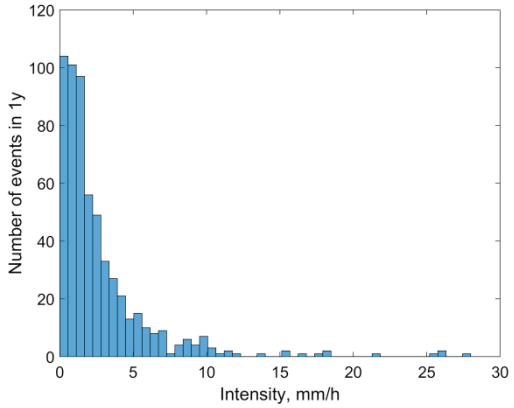

Figure 4. Example histogram of 1-h rainfall intensities simulated for a 1-year period.

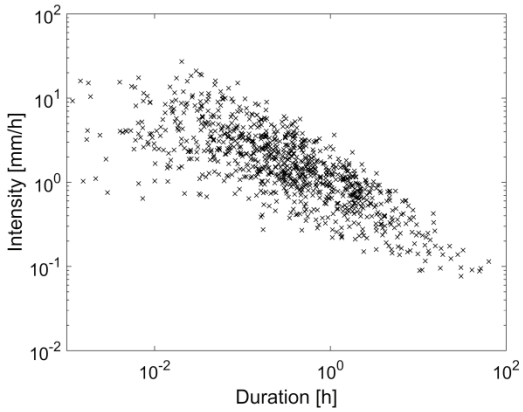

Figure 5. Joint distribution of rainfall intensity and durations for simulated rainfall events over a 1-year period.

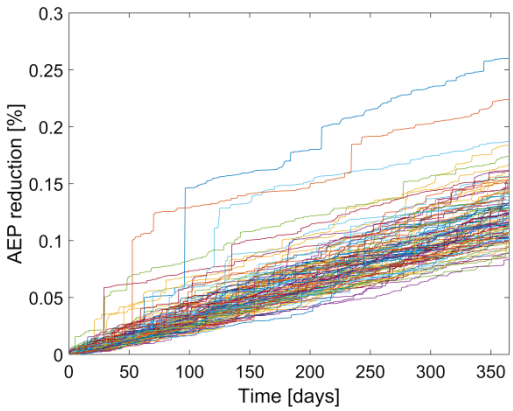

Figure 6. LEE progression expressed as reduction in annual energy production. Results from 100 1-year Monte Carlo simulations.

3.3. Damage growth rate for trailing edge cracks

The suggested computation of trailing edge damage growth rates is based on the assumption that the crack grows in a stable fashion and the crack length increment is a function of the load magnitude, a behaviour which can be described by the Paris-Erdogan crack propagation law [9]. In particular, the crack growth rate described by the Paris-Erdogan law can be related to the strain energy release rates arising from material deformation at the crack tip [10]:

$$\frac{\mathrm{d}a}{\mathrm{d}N} = B(\Delta G)^d \tag{4}$$

where $\mathrm{d}a/\mathrm{d}N$ is the crack growth as function of number of load cycles, B and d are empirical, material-related constants, and $\Delta G = G_{\max} - G_{\min}$ is a strain energy release rate (SERR) dependent on the load range, and on section geometry and compliance. In [11] a comprehensive Finite-Element Analysis investigation of the trailing edge bond behaviour is carried out, and SERRs are computed for a trailing edge crack as function of the loading direction and magnitude. In the present study, the

computation of SERR as function of loading direction and load magnitude is adapted from [11]. The load magnitude is given in a normalized fashion, as the ratio between the resultant external load on the cross section, and the extreme design load for the same section. Figure 7 illustrates the total SERR computed by summing the different crack opening modes: $G_{tot} = G_I + G_{II} + G_{III}$, where G_I, G_{II} and G_{III} are crack opening, in-plane shear, and out-of-plane shear modes respectively. The SERR values shown on Figure 7 are computed for cycles with constant direction, which has to be extended to accommodate multiple loading directions. Here a simple approach is adopted, utilizing the observation that substantial strain energy release only appears in a narrow range of load directions, centered at 110deg and 250deg angles. The section out-of-plane bending moment components (M_x, M_y) computed from an aeroelastic load simulation tool are thus rotated into a coordinate system aligned with the critical loading direction. Then load cycles are counted using the rainflow algorithm, and the cycle ranges are inserted as ΔG in Equation (4). The values of the material parameters B and d are taken as defined in [10], where $\log B \approx -52.516 + 28.058(1 - G_{II}/G_{tot})^{0.35}$, and $d \approx 1.885 + 2.255(G_{II}/G_{tot})^{1.885}$. Applying Equation (4) to the cycles counted in a 10-minute load simulation results in a set of crack increments. The total crack growth over a single load realization, here denoted as $\mathrm{d}a/\mathrm{d}t$, is the sum of the crack increments.

Now, the dependence of $\mathrm{d}a/\mathrm{d}t$ on the environmental conditions can be studied by carrying out multiple load simulations over different conditions. In the present study this procedure is carried out for the DTU 10MW reference wind turbine [12] using the HAWC2 aeroelastic simulation tool [13]. A large number of simulations are carried out with varying wind speed, turbulence intensity and wind shear. For each simulation, the estimated crack growth $\mathrm{d}a/\mathrm{d}t$ is computed for a cross section at 15m from the blade root. For the computation of SERRs, the section resultant bending moment is normalized with a cross section ultimate design load value of 25.47MNm [12]. The relation between $\mathrm{d}a/\mathrm{d}t$, wind speed, turbulence, and wind shear is mapped by means of a surrogate model based on a Polynomial Chaos Expansion, following the procedure described in details in [14]. The resulting response surface is plotted on Figure 8.

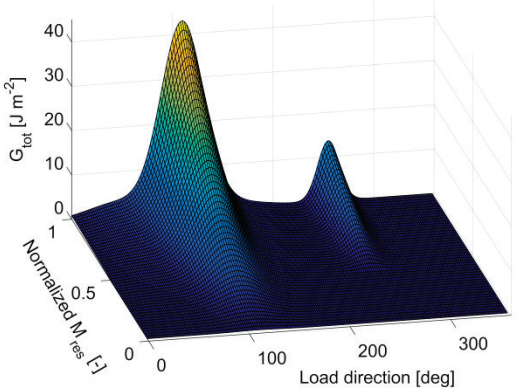

Figure 7. Total strain energy release rates as function of loading direction and magnitude.

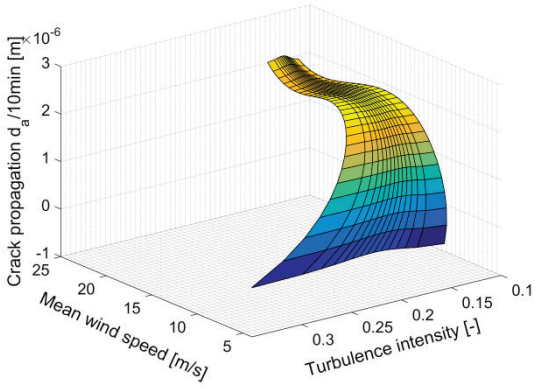

Figure 8. Response surface for the 10-minute crack growth rates as function of mean wind speed and turbulence.

Finally, 100 realizations of 1-year wind speed time histories are generated with a Fourier simulation using a wind speed spectrum based on 20 years of wind speed measurements at a coastal site in Denmark. This approach retains the autocorrelation exhibited by real-world wind time histories, and allows for realization-to-realization variations in the annual mean wind speed. For each wind speed time history, corresponding random turbulence and wind shear time histories are generated using a Log-normally distributed turbulence with IEC class B, and Normally distributed wind shear exponent with mean equal to 0.1 and standard deviation equal to $1/U$, where U is the wind speed.

Combining the time histories of environmental conditions with the surrogate model for $\mathrm{d}a/\mathrm{d}t$ results in a Monte Carlo-type simulation of time histories of crack propagation. This is shown on Figure 9.

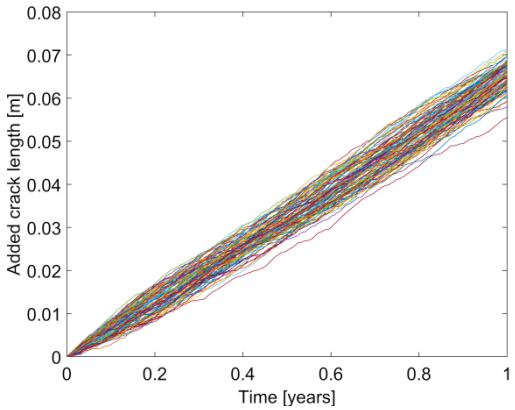

Figure 9. Results from a Monte Carlo simulation with 100 realizations of crack growth over 1 year periods.

4. Model updating and model uncertainties

In the above, damage increments were mapped to the environmental conditions using relatively simple models. This mapping will represent some sort of analytical relationship which may be of the form

$$\Delta D(\mathbf{X}) = a_1 g(X_1, \theta_1) + a_2 g(X_2, \theta_2) + a_{12} g(X_1, X_2, \theta_{12}), \ldots \quad (5)$$

where a_x and θ_x are parameters, and $g(X, \theta)$ are some simple functions of one or more components of $\mathbf{X}$. The values of a and θ will reflect the underlying models used to estimate damage growth rates, and can be associated with high uncertainty. Given that repeated inspections are carried out which allow for establishing some measured estimates of $\Delta D(\mathbf{X})$, the damage growth model may be enhanced by updating the parameter values based on the observations. This can be done using the Bayesian updating technique [15], where a posterior (updated) estimation of the model parameters is obtained by finding the parameter values maximizing the likelihood of the observations, whilst the initial parameter estimates are utilized as the prior distribution in the Bayesian updating formula.

There are a number of uncertainties associated with different models which propagate through the analysis steps. These uncertainties will affect the risk and cost estimates, especially for the problem of estimating failure probabilities, where the variance of the modelled quantities plays a major role. Therefore, in the present study the uncertainties are taken into account when computing the probability of failure due to a trailing edge crack. The majority of uncertainty sources considered are common for most wind energy-related problems [16]: the exposure uncertainty X_{exp} (uncertainty in environmental conditions), the crack-propagation model uncertainty X_{cp}, statistical uncertainty due to limited number of simulations, X_{st}, and X_d, uncertainty in the critical crack size. An uncertainty accounting for possible spatial variation in material properties leading to non-constant crack propagation rate, X_{mat}, is also considered. The probability distributions of the uncertainty variables are listed in Table 1.

Table 1. Uncertainty variables a trailing edge crack growth analysis.

Variable names	Distribution	Mean	c.o.v.
X_d	Log-normal	1	0.1
X_{st}	Log-normal	1	0.05
X_{exp}	Log-normal	1	0.1
X_{cp}	Log-normal	1	0.15
X_{mat}	Log-normal	1	0.05

5. Example risk assessments

In the following, the damage growth models discussed in Section 3 are used to carry out example risk assessments for a trailing edge crack growth problem and for the progression of LEE. For evaluating the risk, the following cost figures are assumed:

- Electricity cost is assumed to be 80EUR/MWh, and the 10MW turbine is assumed to have capacity factor of 0.4;
- The cost of blade replacement is $C_{replace} = 5$mEUR, and it takes 72h to replace;
- The cost of blade repair in scheduled service campaign is $C_{repair} = 2000\text{EUR} + 4000a$, where a is the crack length;
- The cost of blade repair in a dedicated service campaign is $C_{repair} = 10000\text{EUR} + 4000a$;
- The lead time is considered 48h, the replacement time 72h, and the repair time is 48h + 24a for extraordinary service and 24h + 24a when done during scheduled service.

For the trailing edge crack problem, the risk associated with three decision scenarios following a crack detection is evaluated: Sc1.1: Immediate intervention – turbine is stopped and a repair is scheduled, Sc1.2: Delayed intervention – the turbine is kept operating until the repair action is ready, and Sc1.3: Repair is planned at the next scheduled service campaign. It is considered that the crack growth does not influence the power production, thus any production losses only take place when the turbine is stopped due to repair or failure. It is also considered that the probability of no deterioration, $P_{\bar{D}} = 0$. This leads to the following risks of each scenario as function of the observed crack length a:

$$
\begin{aligned}
RSc1.1(a) &= C_{repair}(a) + C_{prod}\left(t_{lead} + t_{repair}(a)\right) \\
RSc1.2(a) &= (1 - P_{FL})\left(C_{repair}(a) + C_{prod}\left(t_{repair}(a)\right)\right) + P_{FL}\left(C_{replace} + C_{prod}\left(t_{lead} + t_{repair}\right)\right) \\
RSc1.3(a) &= (1 - P_{FS})\left(C_{repair}(a) + C_{prod}\left(t_{repair}(a)\right)\right) + P_{FS}\left(C_{replace} + C_{prod}\left(t_{lead} + t_{repair}\right)\right)
\end{aligned} \tag{6}
$$

where $P_{FL} = P\left(t_{fail} \le t_{lead}\right)$ and $P_{FS} = P\left(t_{fail} \le t_{service}\right)$.

To complete the analysis, we need to compute P_{FL} and P_{FS}. This is done using the crack growth model described in Section 3, supplemented with the uncertainty variables given in Table 1. The problem is formulated as a structural reliability analysis with the following limit state equation:

$$g(a(t), \mathbf{X}) = a_{cr}X_d - a_0 - a(t)X_{st}X_{exp}X_{cp}X_{mat} \tag{7}$$

where a_0 is the crack size at the time of inspection, and a_{cr} is the estimated critical crack size. Failure is indicated when $g(a(t), \mathbf{X}) \le 0$. Equation (7) is evaluated using a Monte Carlo simulation and the estimates of the distribution of $a(t)$ shown on Figure 9, resulting in an evaluation of the probability of failure as function of time. These failure probabilities are shown on Figure 10 for three different crack sizes. The accompanying estimation of the probability distribution of t_{fail} for different initial crack sizes is shown on Figure 11. Now, the risk associated with the events considered can be placed in the risk matrix (Figure 1) and thus categorized according to severity. For example, the probability of a 0.4m crack progressing to ultimate failure within 1y is $4 \cdot 10^{-6}$, and the consequence is in the order of 10^6 EUR, which places the scenario in a risk category 3 (Figure 1, denoted as "0.4m"). On the other hand, for a 0.6m crack the estimated probability of failure within 1y is 13%, which, accompanied with the same consequences, places the scenario in risk category 5. Another interesting result from the computations is the plot of crack size vs. risk for the three scenarios, which is shown on Figure 12. It is clear that the optimal decision depends on the observed crack size. For small cracks the risk is governed by the time and cost for repairs. At larger crack sizes the probability of ultimate failure increases, and despite still being small, it is associated with a significant consequence, which makes the possibility of failure a dominating factor for large crack sizes.

A similar risk assessment is now carried out for the case with LEE. The main difference with the crack growth case is that for the problem with LEE it is considered that there will be no need for blade

replacement, and all scenarios involve blade repairs. This also means that the decision for immediate stop in case of damage detection is obsolete and can be disregarded. Three scenarios are considered: schedule a repair as soon as possible, repair after 6 months, and repair after 1 year. For simplicity, the same repair costs as function of damage size are adopted as the ones used for the crack growth problem. The estimates of the risks associated with these scenarios are plotted on Figure 13. Just as in the case with crack propagation, the damage extent at time of inspection affects the optimal decision.

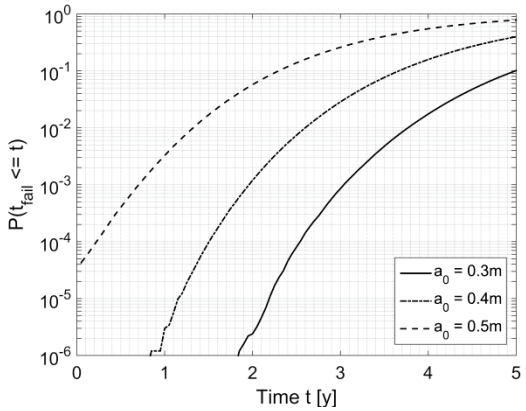

Figure 10. Assessment of the probability for a crack with initial size a_0 to reach the critical size a_{cr} before a given time t.

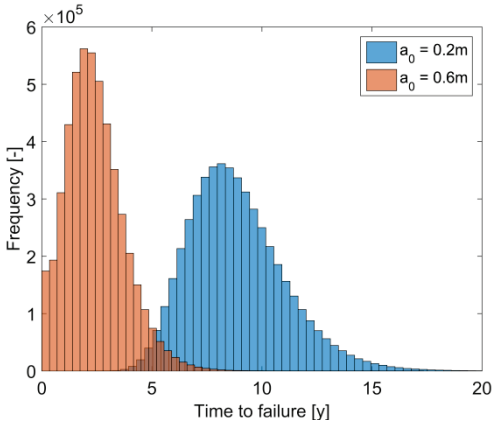

Figure 11. Distributions of estimated time for crack progression from initial size a_0 to a_{cr} for two values of a_0.

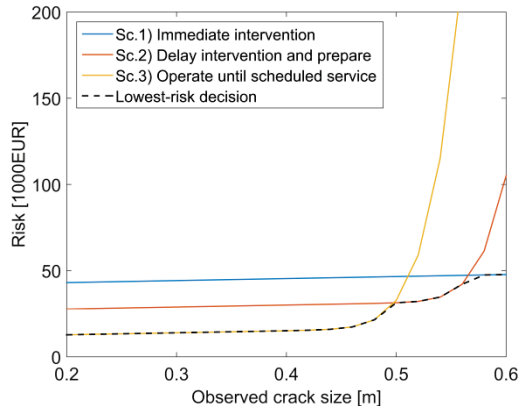

Figure 12. Estimated risk as function of trailing edge crack size for three mitigation scenarios. Dashed black line indicates optimal decision.

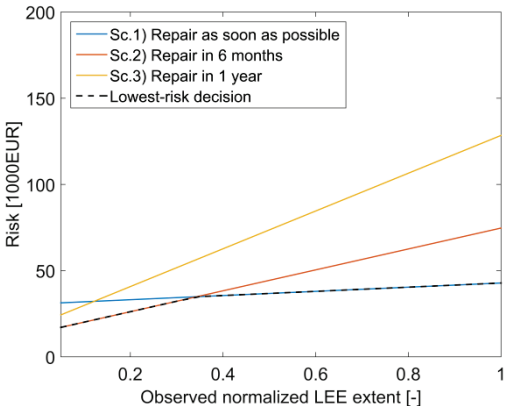

Figure 13. Estimated risk as function of LEE extent for three different mitigation scenarios. Dashed black line indicates optimal decision.

6. Discussion and conclusions

The present study provided a risk-based procedure for assessment and severity categorization of observed wind turbine blade damage. Risk estimates were obtained for two example problems, considering various scenarios for progression and mitigation of a trailing edge crack and leading edge erosion damage. The results demonstrated that the optimal corrective action will depend on the extent of the damage, and the risk assessment can be used to identify the most cost-effective alternative. The risk figures provide an objective, quantitative measure of the severity of a particular damage, and therefore can serve as the basis for damage severity categorization. The categories can represent ranges of risk values, but an alternative definition could define a category as a range of damage sizes where a given decision scenario is most cost-effective.

The procedure relies on model-based estimation of damage progression rates, but in the case of repeated observations over long periods the model parameters may be updated based on evidence. Thus, a realistic usage scenario could start with model-based damage progression rates, which are then gradually updated over a few years as more evidence becomes available.

It should be noted that the models used in the present study to compute the damage increments are for demonstration purposes and based on sources from literature. The results are example, normalized estimations of the damage increments. When implementing these procedures on a given turbine, it will be necessary to re-calibrate these models for the specific turbine design using tests or high-fidelity models.

Acknowledgements

This publication is supported financially by the Innovation Fund Denmark project DARWIN, grant no. 6151-00020B. The support is greatly appreciated.

References

[1] Nielsen, J.S., Sørensen, J.D. (2011) On risk-based operation and maintenance of offshore wind turbine components. *Reliability engineering & system safety* **96**(1), 218-229.
[2] Nielsen, J.S., Sørensen, J.D. (2017) Bayesian estimation of remaining useful life for wind turbine blades. *Energies* **10** (5), article nr. 664.
[3] Kaplan, S., Garrick, B. J. (1981), On The Quantitative Definition of Risk. *Risk Analysis* **1**, 11–27. doi:10.1111/j.1539-6924.1981.tb01350.x
[4] Torsional Stiffening of Wind Turbine Blades – Mitigating leading edge damages: *EUDP project 64013-0115 – Final report*. Bladena.
[5] Bech, J. I., Hasager, C. B., and Bak, C. (2018) Extending the life of wind turbine blade leading edges by reducing the tip speed during extreme precipitation events. *Wind Energ. Sci. Discuss.*, https://doi.org/10.5194/wes-2017-62, in review.
[6] Best, A. C. (1950) The size distribution of raindrops. *Q. J. R. Meteorol. Soc.* **76,** 16–36.
[7] Jones, D. M. a & Sims, A. L. (1978) Climatology of instantaneous rainfall rates. *J. Appl. Meteorol.* **17,** 1135–1150.
[8] Koutsoyiannis, D., Kozonis, D. & Manetas, A. (1998) A mathematical framework for studying rainfall intensity-duration-frequency relationships. *J. Hydrol.* **206,** 118–135.
[9] Paris, P., & Erdogan, F. (1963). A Critical Analysis of Crack Propagation Laws. *Journal of Basic Engineering*, **85**(4), 528.
[10] Kenane, M., & Benzeggagh, M. L. (1997) Mixed-mode delamination fracture toughness of unidirectional glass/epoxy composites under fatigue loading. *Compos. Sci. Technol.* **3538,** 597–605.
[11] Haselbach, P. U., Eder, M. A. & Belloni, F. (2016)A comprehensive investigation of trailing edge damage in a wind turbine rotor blade. *Wind Energy* **19,** 1871–1888.
[12] Bak, C. *et al.* (2013) Description of the DTU 10 MW Reference Wind Turbine. *DTU Wind Energy Report-I-0092* 1–138. doi:10.1017/CBO9781107415324.004
[13] Larsen, T. J., and Hansen, A. M. (2014) How 2 HAWC2, the user's manual, *Risø-R-1597(ver.4-5)(EN)*. Risø National Laboratory, Technical University of Denmark.
[14] Dimitrov, N., Kelly, M., Vignaroli, A., and Berg, J. (2018) From wind to loads: wind turbine site-specific load estimation using databases with high-fidelity load simulations, *Wind Energ. Sci. Discuss.*, https://doi.org/10.5194/wes-2018-18, in review.
[15] Box, G. E. P., Tiao, G. C. (1973) *Bayesian Inference in Statistical Analysis*. Addison Wesley, Chicago.
[16] Tarp-Johansen, N. (2003) Examples of Fatigue Lifetime and Reliability Evaluation of Larger Wind Turbine Components, *Risø-R-1418*. Risø National Laboratory, Technical University of Denmark.